

Chapter 4

Study on mobility enhancement in MOVPE-grown AlGaN/ AlN/GaN HEMTs using a thin AlN interfacial layer

4.1. Introduction

4.1.1. Foreword

HEMTs based on AlGaN/GaN heterostructures are very promising electronic devices for high-power and high-frequency applications due to their superior material features, and their excellent performance has recently been demonstrated not only in high-power microwave devices but also in high-power and/or high-speed switching devices, as presented in Chapter 1. The recent progress in these devices has been sufficient to show that GaN and related alloys will play a significant role in the future development of high-power and high-frequency electronic devices.

One of the current researches concerning GaN-based HEMTs has been on improving their carrier transport properties of 2DEG. Different growth methods, different substrates and novel structures have been tried to achieve large 2DEG density and high electron mobility [1-8]. Recently, it has been reported that modified AlGaN/AlN/GaN structures, which employ a thin AlN interfacial layer between the AlGaN and GaN layers, show higher 2DEG properties than those of conventional AlGaN/GaN structures [1,2]. This is reported to be a result of the reduction of alloy disorder scattering due to the suppression of carrier penetration from the GaN channel into the AlGaN layer [1,2,9]. In order to realize the application of AlGaN/AlN/GaN

structures to electronic devices, it is necessary to understand their basic structural and electron transport properties in detail. In this chapter, we have investigated the effect of the thin AlN interfacial layer on the 2DEG properties in AlGa_N/AlN/GaN structures using samples grown on 100-mm-diameter sapphire substrates by MOVPE. HEMTs were also fabricated using these epitaxial wafers and their DC performance was characterized.

4.1.2. Features of AlGa_N/AlN/GaN HEMT structures

Recently, modified AlGa_N/GaN HEMT structures with a thin AlN interfacial layer has been proposed by Shen *et al.* [2]. They reported that an AlGa_N/AlN/GaN HEMT structure with a 1-nm-thick AlN interfacial layer grown on a SiC substrate showed a high room-temperature Hall mobility of 1540 cm²/Vs with a large 2DEG density of $1.48 \times 10^{13}/\text{cm}^2$ [2]. This high performance is reported to be a result of the reduction of alloy disorder scattering due to the suppression of carrier penetration from the GaN channel into the AlGa_N layer [1,2,9]. They also reported that a 0.7- μm -gate length HEMT based on the AlGa_N/AlN/GaN structure exhibits excellent DC and RF device performances such as an extrinsic transconductance of approximately 200 mS/mm, a drain current density of approximately 1 A/mm with a pinchoff voltage of -3.5 V and an output power density of 8.4 W/mm at an operation frequency of 8 GHz [2].

Figures 4.1(a) and 4.1(b) shows conduction-band diagrams of a conventional AlGa_N/GaN structure and an AlGa_N/AlN/GaN structure, respectively [2]. Figure 4.1(b) shows that the insertion of a thin AlN layer produces a larger effective ΔE_C , which is defined as conduction-band discontinuity between AlGa_N and GaN at both sides of the thin AlN layer. The increase in effective ΔE_C is due to polarization-induced dipole in the AlN layer. The primary advantage of the insertion of the AlN layer is the decrease in alloy disorder scattering leading to an increase in 2DEG mobility. This is because the electron penetration into the AlGa_N layer is reduced due to the higher ΔE_C , and also the binary AlN at the interface has no

alloy disorder scattering. As reported in Ref. 1, the decrease in alloy disorder scattering improves low-temperature 2DEG mobility. In addition, considering the large 2DEG densities attainable in this materials system, alloy disorder scattering can play a significant role in room temperature mobility values. Meanwhile, it can be expected that the large ΔE_C results in the increase in 2DEG concentration due to the suppression of the carrier penetration from the GaN channel into the AlGaN layer.

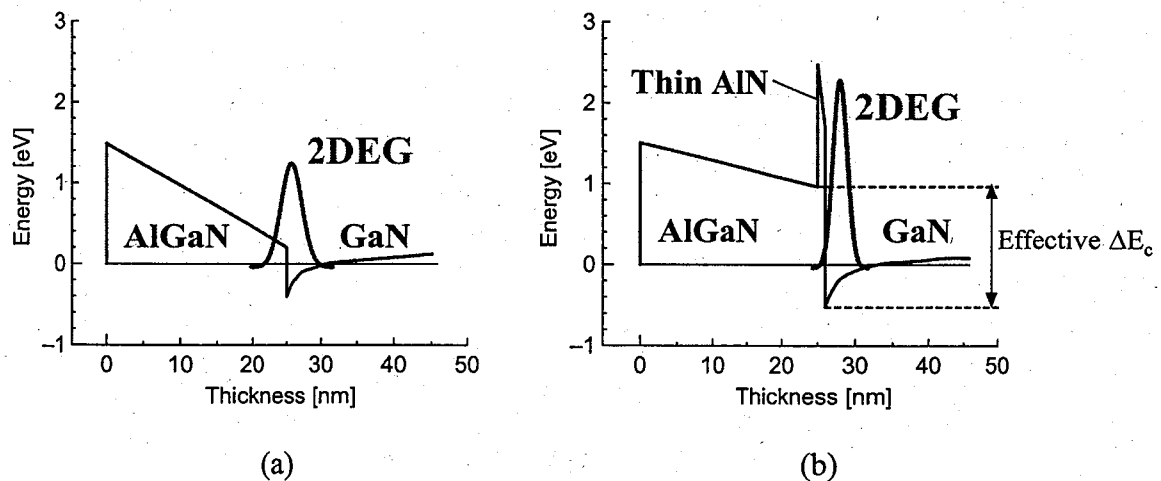


FIG. 4.1. Schematic conduction band diagram of: (a) conventional AlGaN/GaN HEMT, (b) novel AlGaN/AlN/GaN HEMT, Dipole in AlN increases the effective ΔE_C .

4.2. Experiment

AlGaN/AlN/GaN structures with AlN interfacial layers of various thicknesses were grown on 100-mm-diameter and 630- μm -thick *c*-face sapphire substrates using a horizontal MOVPE system (Taiyo Nippon Sanso, SR-4000). Trimethylgallium (TMG), trimethylaluminum (TMA) and ammonia (NH_3) were used as Ga, Al and N sources, respectively, and monosilane (SiH_4) was used as the n-type dopant. Figure 4.2 schematically shows the cross section of MOVPE-grown samples. The AlGaN layer consists of, from top to bottom, a 3-nm-thick undoped $\text{Al}_{0.26}\text{Ga}_{0.74}\text{N}$ layer, a 15-nm-thick Si-doped $\text{Al}_{0.26}\text{Ga}_{0.74}\text{N}$ layer with the doping level of approximately $5 \times 10^{18}/\text{cm}^3$ and a 7-nm-thick undoped $\text{Al}_{0.26}\text{Ga}_{0.74}\text{N}$ layer. The

GaN layer thickness was maintained at 3 μm . The growth conditions of the GaN layers have been optimized to have a resistivity of higher than $1 \times 10^6 \Omega\text{cm}$ over the entire 100-mm-diameter epitaxial wafers. The AlN interfacial layers were grown to have thicknesses of 0, 0.5, 0.75, 1.0, 1.25 and 1.5 nm according to the growth rate. The MOVPE-grown wafers were characterized by various techniques including Hall effect measurement, the contactless eddy current method, Hg-probe capacitance-voltage ($C-V$) measurement, atomic force microscopy (AFM) and cross-sectional transmission electron microscopy (TEM).

The fabrication of HEMTs was performed using a conventional photolithographic lift-off method. Source and drain patterns were accomplished by the evaporation of Ti/Al/Ni/Au (25/75/20/55 nm), and were subsequently annealed at a temperature of 850°C for 30 s in nitrogen atmosphere. The gate Schottky contacts were formed by the evaporation of Pd/Ti/Au (40/20/60 nm). Device isolation was accomplished by mesa dry etching down to GaN layers by RIE. Electron-beam-evaporated SiO₂ films were used for device passivation. The gate width (W_g) and the gate length (L_g) were 15 μm and 1.5 μm , respectively. Current-voltage ($I-V$) characteristics were measured using a semiconductor parameter analyzer.

i-Al _{0.26} Ga _{0.74} N (3 nm)
n-Al _{0.26} Ga _{0.74} N (15 nm) (N _d : $5 \times 10^{18}/\text{cm}^3$)
i-Al _{0.26} Ga _{0.74} N (7 nm)
AlN (0–1.5 nm)
i-GaN (3 μm)
GaN LT-BL (25 nm)
c-face sapphire (630 μm)

FIG. 4.2. Cross section of MOVPE-grown samples.

4.3. Results and discussion

4.3.1. Characterization of MOVPE-grown epilayers

Figures 4.3(a) and 4.3(b) show plots of Hall mobilities (μ_{Hall}) and sheet resistances (ρ_s) measured at room temperature (RT) and 77 K, respectively, for a series of samples with AlN layer thicknesses of 0, 0.5, 0.75, 1.0, 1.25 and 1.5 nm. From Figures 4.3(a) and 4.3(b), it is clear that Hall mobility and sheet resistance vary with the thickness of the AlN interfacial layer, and that these have an optimum value for a certain AlN layer thickness. Highly enhanced Hall mobilities with low sheet resistances, such as 1770 cm^2/Vs with 365 $\Omega/\text{sq.}$ at RT and 7260 cm^2/Vs with 87 $\Omega/\text{sq.}$ at 77 K (2DEG density $n_s = 1.0 \times 10^{13}/\text{cm}^2$), were observed for a sample with an optimum AlN layer thickness of 1.0 nm compared with those of a sample without the thin AlN interfacial layer ($\mu_{\text{Hall}} = 1287 \text{ cm}^2/\text{Vs}$ at RT and 3998 cm^2/Vs at 77K, $\rho_s = 539 \Omega/\text{sq.}$ at RT and 174 $\Omega/\text{sq.}$ at 77K, $n_s = 0.9 \times 10^{13}/\text{cm}^2$).

Figure 4.4 shows the temperature dependence of the Hall mobilities for the AlGaIn/AlN/GaN structure with the 1-nm-thick AlN interfacial layer. For comparison, Figure 4.4 also shows the results of the AlGaIn/GaN structure. From this figure, it is clear that the saturation of Hall mobilities at low temperatures, in which the alloy disorder and/or interface roughness are the dominant scattering processes [1], is markedly reduced in the case of the AlGaIn/AlN/GaN structure compared with that in the case of the AlGaIn/GaN structure. This result indicates that the dominant scattering processes at low temperatures are significantly screened by the insertion of the thin AlN interfacial layer. The Hall mobility of the AlGaIn/AlN/GaN structure reaches a very high value of approximately 8200 cm^2/Vs at 15 K.

Figure 4.5(a) shows the in-wafer contour mapping of the sheet resistance for the AlGaIn/AlN/GaN structure with a 1-nm-thick AlN interfacial layer measured at 81 points in the wafer by the contactless eddy current method. Figure 4.5(b) shows the line scan distributions of the sheet resistance (ρ_s), Hall mobility (μ) and 2DEG density (n_s) measured by the Hall effect

measurement. As seen in these figures, a relatively good in-wafer electrical uniformity is obtained for this sample. From Figure 4.5(a), the average sheet resistance and its in-wafer standard deviation were measured to be 371 $\Omega/\text{sq.}$ and 3.5%, respectively. Also, Figure 4.5(b) shows that the sheet resistance measured by the Hall effect measurement (365 $\Omega/\text{sq.}$) was approximately consistent with that measured by the eddy current method (371 $\Omega/\text{sq.}$). Therefore, it can be speculated that a high Hall mobility of over 1700 cm^2/Vs were uniformly realized over the entire 100-mm-diameter epitaxial wafer. We understand that these electrical homogeneities indicate the structural homogeneities, which means that the thin AlN interfacial layer is uniformly grown across the entire 100-mm-diameter wafer.

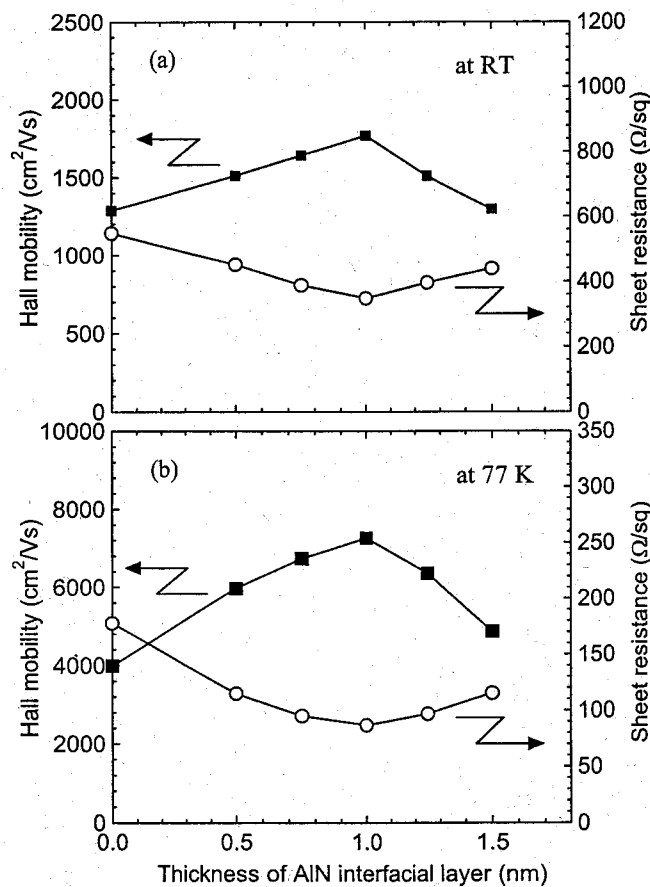


FIG. 4.3. Plots of mean sheet resistances and Hall mobilities measured (a) at room temperature (RT) and (b) at 77 K, respectively, for a series of AlGaIn/AlN/GaN structures with AlN layer thicknesses of 0, 0.5, 0.75, 1.0, 1.25 and 1.5 nm.

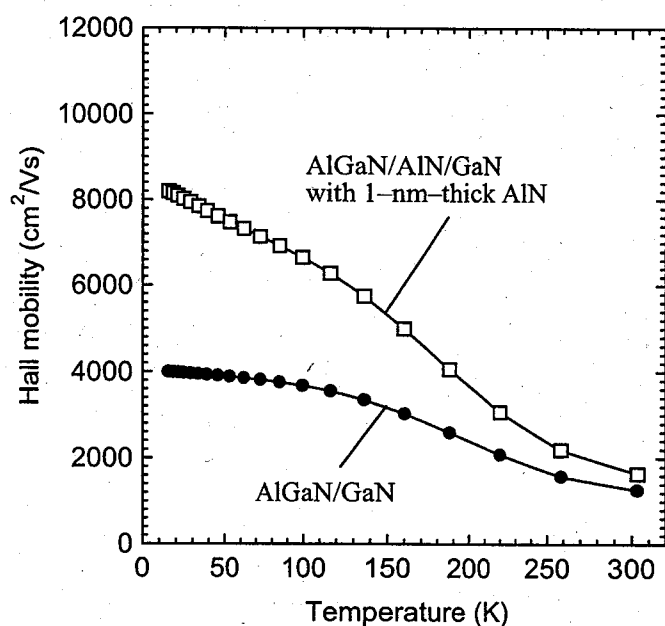


FIG. 4.4. Temperature dependence of Hall mobility for MOVPE-grown epitaxial wafers.

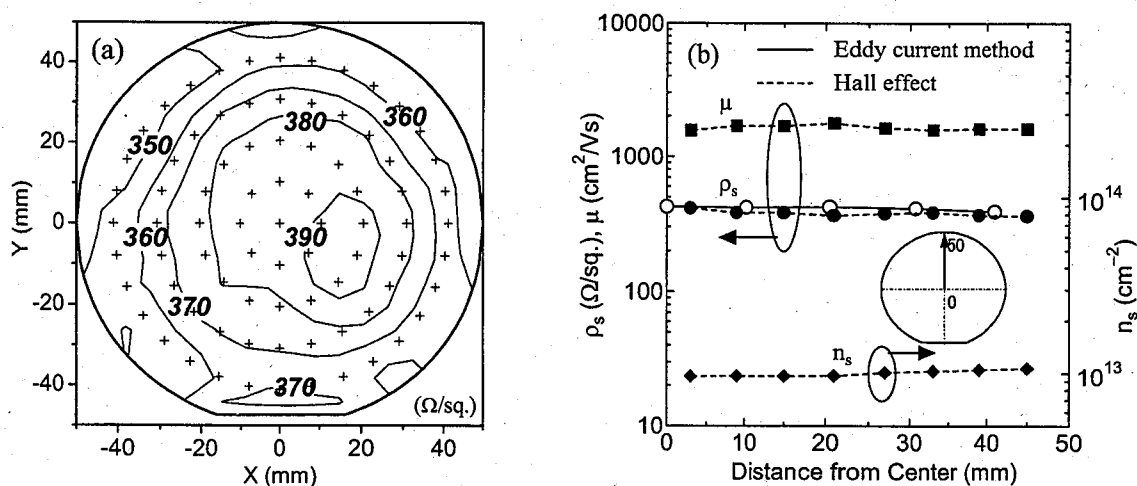


FIG. 4.5. In-wafer sheet resistance mapping of (a) a 100-mm-diameter MOVPE-grown AlGaIn/AlN/GaN structure with a 1-nm-thick AlN interfacial layer measured by the contactless eddy current method. Crosses (+) represent the points of measurement. (b) Line scan distribution of sheet resistance (ρ_s), Hall mobility (μ) and 2DEG density (n_s) across the 100-mm-diameter MOVPE-grown AlGaIn/AlN/GaN structure with a 1-nm-thick AlN interfacial layer measured by the Hall effect measurement (dashed lines) and the eddy current method (solid lines).

Figure 4.6(a) shows typical results of C - V profiling for the AlGa_N/AlN/GaN structure with the 1-nm-thick AlN interfacial layer measured by the Hg-probe C - V method. In this figure, the result for the conventional AlGa_N/GaN structure is also shown. As seen in this figure, the AlGa_N/AlN/GaN structure shows a sharp 2DEG peak around the thin AlN interfacial layer, while the AlGa_N/GaN structure shows a relatively broad 2DEG distribution and its penetration into the AlGa_N layer. The peak 2DEG density of the AlGa_N/AlN/GaN structure was three to four times larger than that of the AlGa_N/GaN structure. This result directly indicates that the thin AlN interfacial layer effectively suppresses carrier penetration into the AlGa_N layer and enhances the confinement of 2DEG in the GaN channel. We can consider that the well-confined 2DEG lead to high mobilities due to the suppression of alloy disorder scattering [1,2,9]. Figure 4.6(b) shows the C - V measured threshold voltages (V_{th}) for AlGa_N/AlN/GaN structures with AlN interfacial layers of various thicknesses. As seen in this figure, the C - V measured V_{th} linearly shifted to negative voltages with increasing the AlN layer thickness. This result roughly indicates that the ΔE_C increases with increasing the AlN layer thickness. This is because the V_{th} of AlGa_N/GaN HEMTs is expressed as: $V_{th} = \phi_B - \Delta E_C - aP_{total} / \epsilon$ [10], where ϕ_B is the Schottky contact barrier height, P_{total} is the sum of the spontaneous polarization charge and piezoelectric charge, a is the thickness of the AlGa_N layer.

Figure 4.7(a) shows a cross-sectional TEM image of an MOVPE-grown AlGa_N/AlN/GaN film, which was grown to have a 1-nm-thick AlN interfacial layer. Correspondingly, Figure 4.7(b) shows a high-resolution cross-sectional TEM image taken around the AlGa_N/AlN/GaN interfaces. As seen in Figure 4.7(a), the thin AlN layer between the GaN and AlGa_N layers is observed as a dark region. This seems to be because the condition of the Bragg diffraction was adjusted not to the crystal parameters of the AlN layer but to those of the GaN and AlGa_N layers, so that the effect of the strain in the AlN layer on the color contrast was enhanced, and the AlN

layer was represented as a dark region in the TEM image. From Figure 4.7(a), it can be observed that the AlN interfacial layer is grown with a thickness of approximately 1 nm, which corresponds to the designed thickness. In addition, Figure 4.7(b) reveals that atoms are almost continuously aligned and well ordered across the interfaces. From these results, it may be concluded that atomically abrupt and flat interfaces are realized in the AlGaN/AlN and AlN/GaN heterointerfaces, which seems to be very important for the realization of good 2DEG properties.

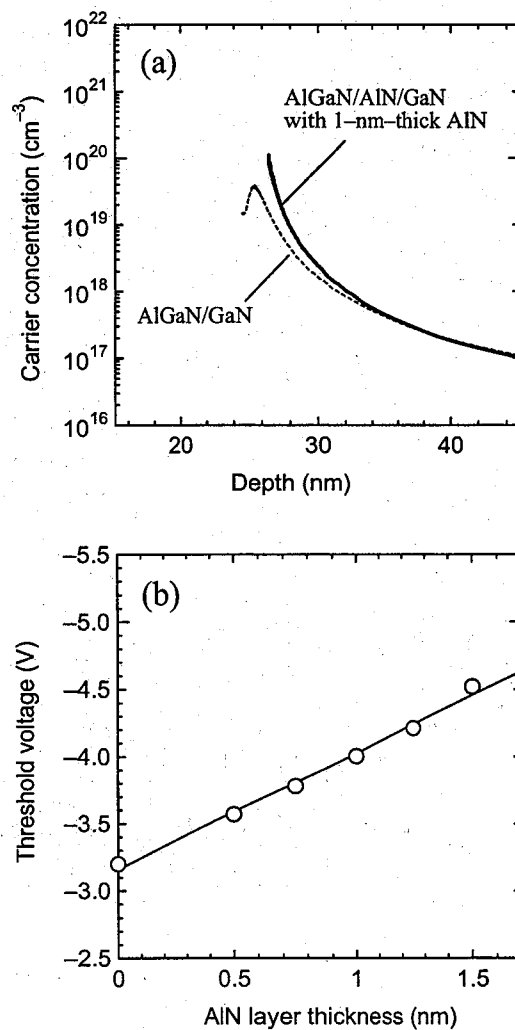


FIG. 4.6 (a) Typical depth profiles of electron densities for MOVPE-grown AlGaN/AlN/GaN and AlGaN/GaN structures measured by the Hg-probe C - V method. (b) C - V measured threshold voltages (V_{th}) for AlGaN/AlN/GaN structures with AlN interfacial layers of various thicknesses.

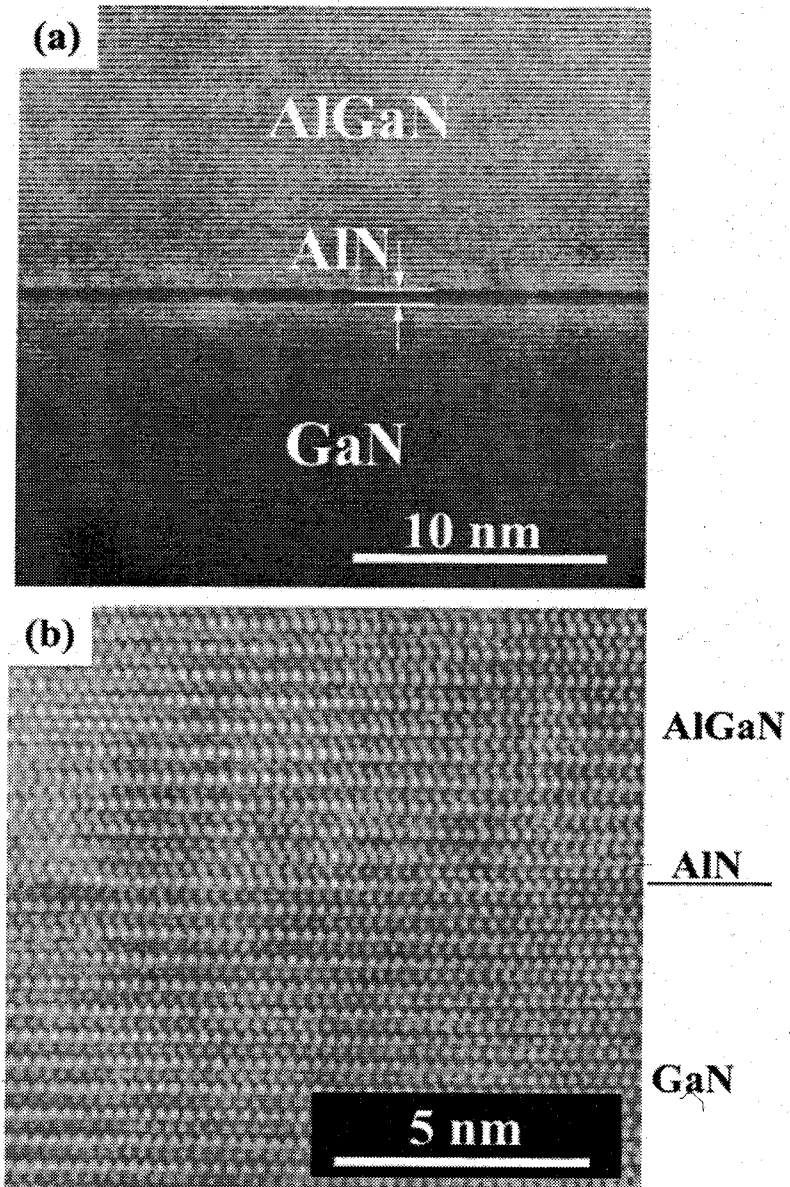


FIG. 4.7. (a) Cross-sectional TEM image of AlGaN/AIN/GaN film and (b) high-resolution cross-sectional TEM image taken around AlGaN/AIN/GaN interfaces.

4.3.2. Consideration for 2DEG properties in AlGaN/AlN/GaN structures

4.3.2.1. 2DEG transport properties in AlGaN/AlN/GaN structures

In order to understand the electron transport properties in AlGaN/AlN/GaN structures, the carrier scattering mechanism was investigated. Various scattering processes, such as polar optical phonons, acoustic phonons, piezoelectric field, alloy disorder, interface roughness and dislocation, were taken into account [11-13] according to the calculation presented in Chapter 3. The mobility related to dislocation scattering (μ_{dis}) was calculated according to the calculation given in Ref. 13, and the dislocation density of $3 \times 10^9/\text{cm}^2$, which has been estimated by TEM observations, were used in this calculation. The mobility related to interface roughness scattering (μ_{IFR}) was characterized by fitting the calculated mobilities to the measured results using two parameters [13]: the root-mean-square roughness height (Δ) and the lateral correlation length (Λ), which were assumed to have same values in both of AlGaN/GaN and AlGaN/AlN/GaN structures ($\Delta = 0.5 \text{ nm}$, $\Lambda = 5.0 \text{ nm}$), in order to focus on the alloy disorder scattering. The other scattering processes were calculated using parameters given in Ref. 11, and these scattering mechanisms are combined according to the expression $1/\mu = \sum_i (1/\mu_i)$, where μ_i represents an individual mobility. The temperature dependences of the individual and combined mobilities are shown in Figure 4.8(a). In Figure 4.8(a), experimental results for MOVPE-grown AlGaN/GaN structures are also shown.

As seen in Figure 4.8(a), the total calculated mobilities, i.e.: the values calculated including all scattering processes, are in good agreement with the experimental results for the MOVPE-grown AlGaN/GaN structure. From Figure 4.8(a), it can be seen that the alloy disorder and interface roughness scattering have strong impacts on the 2DEG mobility in AlGaN/GaN structures. We also calculated total mobilities excluding alloy disorder scattering, and the calculated results are shown in Figure 4.8(b), in which the experimental results of the

AlGaN/GaN structure and the AlGaN/AlN/GaN structure with the 1-nm-thick AlN interfacial layer are also shown. As seen in this figure, the calculated results excluding alloy disorder scattering are in good agreement with the experimental results for the MOVPE-grown AlGaN/AlN/GaN structure. These agreements indicate that the AlN interfacial layer can significantly enhance the 2DEG mobility due to the reduction of alloy disorder scattering. This is presumably because carrier penetration from the GaN channel into the AlGaN alloy was effectively suppressed by the insertion of the AlN interfacial layer into the AlGaN/GaN heterointerface [1,2,9]. Further investigations, where changes in the interface roughness due to the insertion of the AlN interfacial layer should be taken into account, are now attempted to understand the 2DEG transport properties in AlGaN/AlN/GaN structures in more detail.

4.3.2.2. Consideration for mobility enhancement in AlGaN/AlN/GaN structures

As presented above, we theoretically as well as experimentally revealed that the 2DEG mobility of AlGaN/GaN structures can be significantly enhanced by using an AlN interfacial layer. This seems because alloy disorder scattering is largely reduced to the extent that alloy disorder scattering can be neglected [1,2,9]. On the other hand, we have also confirmed that the Hall mobilities of AlGaN/AlN/GaN structures have an optimum value for a certain AlN layer thickness. The mechanism of this phenomenon is discussed in this section.

We understand that the insertion of an AlN interfacial layer into AlGaN/GaN structures has two significant roles. First, the increased ΔE_C enhances the 2DEG confinement in the GaN channel. The penetration depth of 2DEG into an AlGaN layer is given by the expression [9]:

$$Z_p = \hbar / \sqrt{2m^* \Delta E_c} . \quad (4.1)$$

This equation indicates that the penetration depth is dependent on the ΔE_C at the interface. In the case of a conventional Al_{0.25}Ga_{0.75}N/GaN structure (corresponding to $\Delta E_C = 0.3$ eV and $Z_p = 0.75$ nm), alloy disorder scattering would be the dominant scattering process.

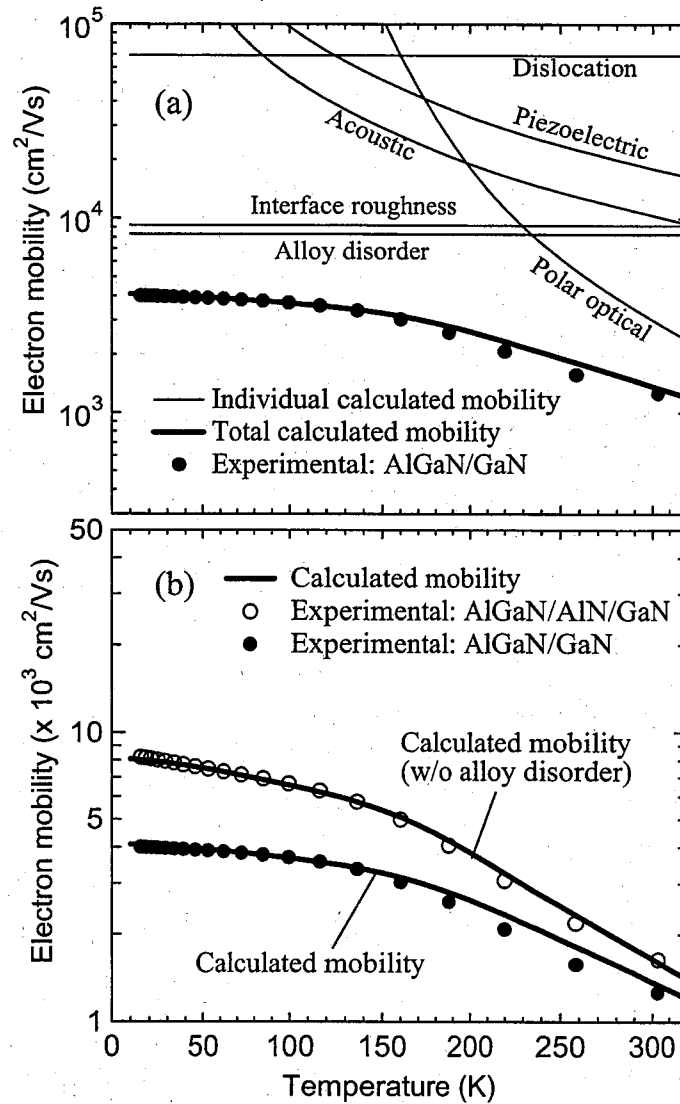


FIG. 4.8 (a) Temperature dependence of electron mobilities in MOVPE-grown AlGaIn/GaN structures on sapphire substrates (\bullet), and calculated mobilities for AlGaIn/GaN structures with consideration of scattering processes due to polar-optical phonons, acoustic phonons, piezoelectric field, interface roughness, dislocation and alloy disorder. Total calculated mobilities mean the values calculated with consideration of all scattering processes. (b) Temperature dependences of electron mobilities in MOVPE-grown AlGaIn/GaN (\bullet) and AlGaIn/AlN/GaN (\circ) structures on sapphire substrates, and total calculated mobilities with and without consideration of alloy disorder scattering.

Second, the binary AlN layer at the interface has no alloy disorder scattering unlike the ternally AlGaIn alloys. The relaxation time for alloy disorder scattering in AlGaIn/GaN structures is related to the Al content x_{Al} in AlGaIn layers as given by the expression [12]:

$$\frac{1}{\tau_{\text{alloy}}} \propto (1 - x_{Al}) \cdot x_{Al} \cdot N_S^2 \cdot \int_{-\infty}^0 \exp(4Z_p \cdot z) dz. \quad (4.2)$$

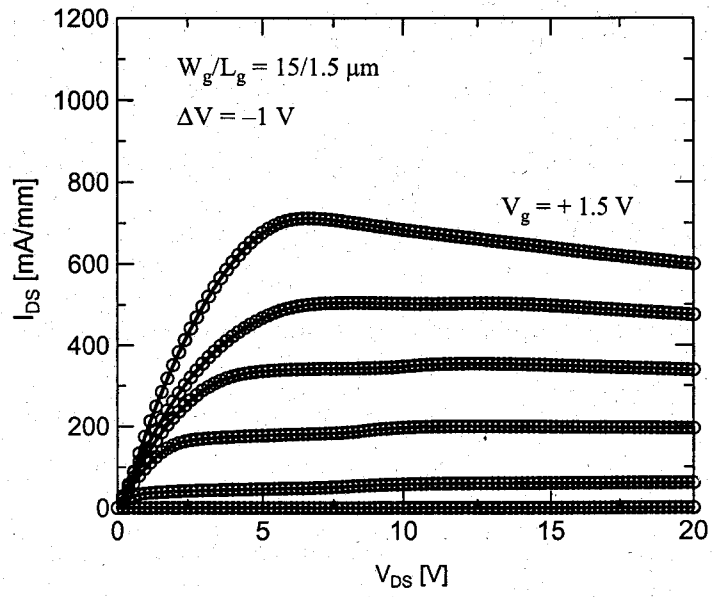
This equation indicates that the effect of alloy disorder scattering on 2DEG mobility should disappear in the case of AlGaIn/AlN/GaN structures (corresponds to $x_{Al} = 1$ and $1/\tau_{\text{alloy}} = 0$) even when the 2DEG penetrates into the AlN layer. In the case when the 2DEG penetrates into the AlGaIn layer across the thin AlN interfacial layer, however, the effect of alloy disorder scattering cannot be neglected. We have confirmed, from C - V study, that the ΔE_C can increase with increasing the AlN layer thickness. This also indicates that the electron penetration depth increases with decreasing the AlN layer thickness. Thus, it can be speculated that the carrier confinement of 2DEG was insufficient for samples with thinner AlN interfacial layers to reduce the effect of alloy disorder scattering on the 2DEG mobility.

On the other hand, it was also observed that the Hall mobilities of AlGaIn/AlN/GaN structures decrease with the increasing the AlN layer thickness to values of thicker than 1 nm. This is presumably due to that the film quality of the AlN interfacial layer degrades with increasing the AlN layer thickness, which may cause a poor interface quality and correspondingly enhances the effect of interface roughness scattering on 2DEG mobility. The 2DEG mobility in AlN/GaN heterostructures has been studied by Smorchkova *et al.* for samples grown by molecular-beam epitaxy [1]. They have reported that 2DEG mobility in AlN/GaN heterostructures decreases with increasing the AlN layer thickness due to the poor film quality. We believe that the film quality in the AlN layers grown on GaN layers is strongly related to the interface quality. This is because the interface and film qualities in those heterostructures seem

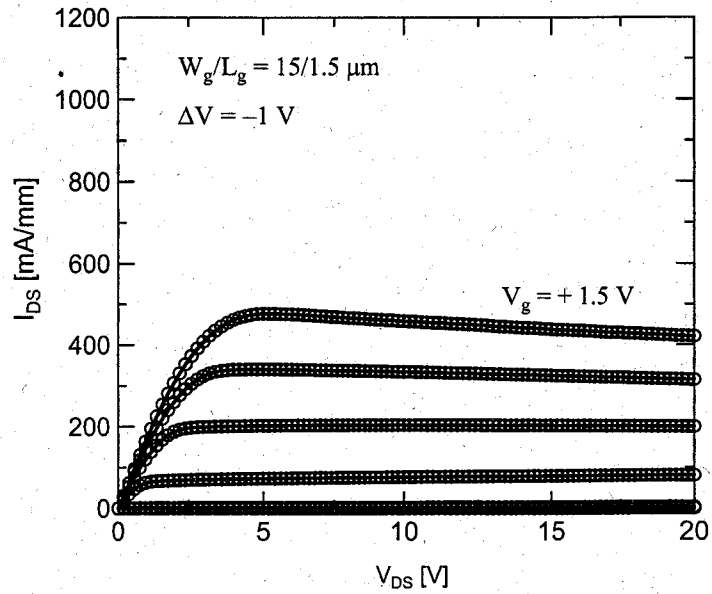
to be related to the structural fluctuation around the heterointerface, which may be attributed to misfit dislocations [14], strain driven three-dimensional growth [15] or partial relaxation [16] yield at the interfaces. Thus it can be speculated that the interface roughness in our MOVPE-grown AlGaIn/AlN/GaN structures also degraded with increasing the AlN layer thickness and enhanced the effect of interface roughness scattering.

4.3.3. Fabrication of HEMTs and their characterization results

HEMTs were successfully fabricated using the present MOVPE-grown epitaxial wafers. Figures 4.9(a) and 4.9(b) show typical drain-source I - V characteristics (I_{DS} - V_{DS}) for 1.5- μ m-gate-length AlGaIn/AlN/GaN HEMTs and AlGaIn/GaN HEMTs. Also, Figures 4.10(a) and 4.10(b) show typical transfer characteristics (g_m - V_{GS}) for AlGaIn/AlN/GaN HEMTs and AlGaIn/GaN HEMTs. As seen in these figures, the fabricated devices exhibited good pinch-off characteristics. DC characteristics of HEMTs fabricated on the present epitaxial wafers are summarized in Table 4.1. It was confirmed that the V_{th} in AlGaIn/GaN HEMTs shifts by approximately 0.8 V toward negative voltages with the insertion of the 1-nm-thick AlN interfacial layer. This is in good agreement with the result obtained by C - V measurements (see Figure 4.6(b)). From Figures 4.9 and 4.10 and Table 4.1, it is clear that AlGaIn/AlN/GaN HEMTs showed higher performance than AlGaIn/GaN HEMTs. A maximum drain-source current density ($I_{DS \text{ max}}$) of as high as 712 mA/mm and a maximum extrinsic transconductance ($g_m \text{ max}$) of as high as 170 mS/mm was observed for 1.5- μ m-gate-length AlGaIn/AlN/GaN HEMTs compared with AlGaIn/GaN HEMTs ($I_{DS \text{ max}} = 477$ mA/mm, $g_m \text{ max} = 138$ mS/mm)(see Figures 4.9 and 4.10 and Table 4.1). From these results, it can be concluded that the electrical properties in AlGaIn/GaN HEMTs are clearly improved by inserting a thin AlN layer into the AlGaIn/GaN heterointerface. The high performance of AlGaIn/AlN/GaN HEMTs seems to be attributed to their excellent 2DEG properties.

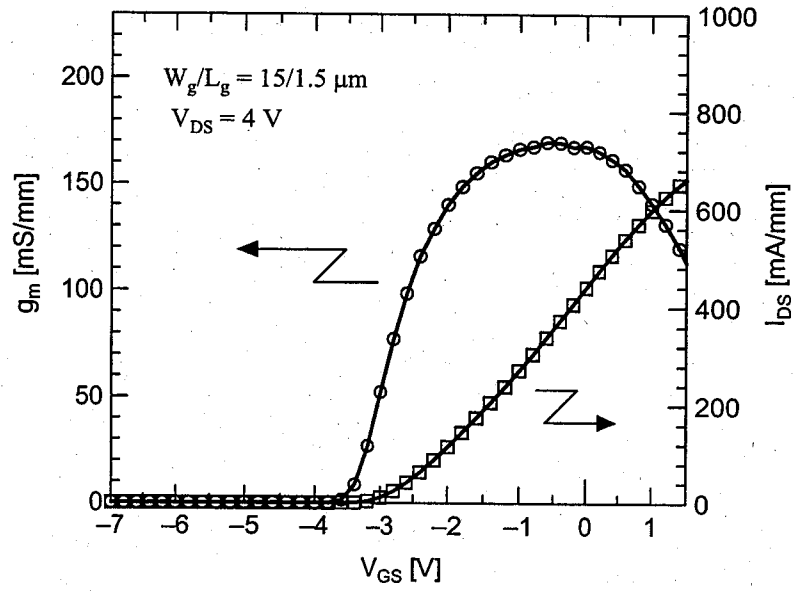


(a)

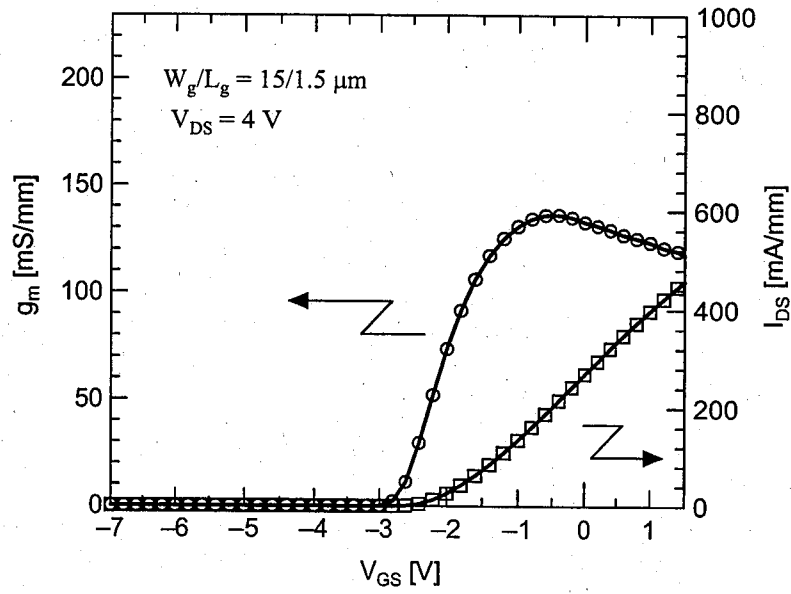


(b)

FIG. 4.9. Typical I_{DS} - V_{DS} characteristics of (a) AlGaIn/GaN HEMTs with a 1-nm-thick AlN interfacial layer and (b) AlGaIn/GaN HEMTs. The gate length (L_g) and the gate width (W_g) were 1.5 μm and 15 μm , respectively.



(a)



(b)

FIG. 4.10. Typical g_m - V_{GS} characteristics ($V_{DS} = 4$ V) of (a) AlGaIn/AlN/GaN HEMTs with a 1-nm-thick AlN interfacial layer and (b) AlGaIn/GaN HEMTs. The gate length (L_g) and the gate width (W_g) were 1.5 μm and 15 μm , respectively.

TABLE 4.1. DC characteristics of AlGaN/AlN/GaN and AlGaN/GaN HEMTs grown on sapphire substrates. The gate length (L_g) and the gate width (W_g) were 1.5 μm and 15 μm , respectively.

Structure	R_s (Ωmm)	V_{th} (V)	$I_{DS\ max}$ (mA/mm)	$g_m\ max$ (mS/mm)
AlGaN/AlN/GaN	2.40	-3.49	712	170
AlGaN/GaN	3.24	-2.71	477	138

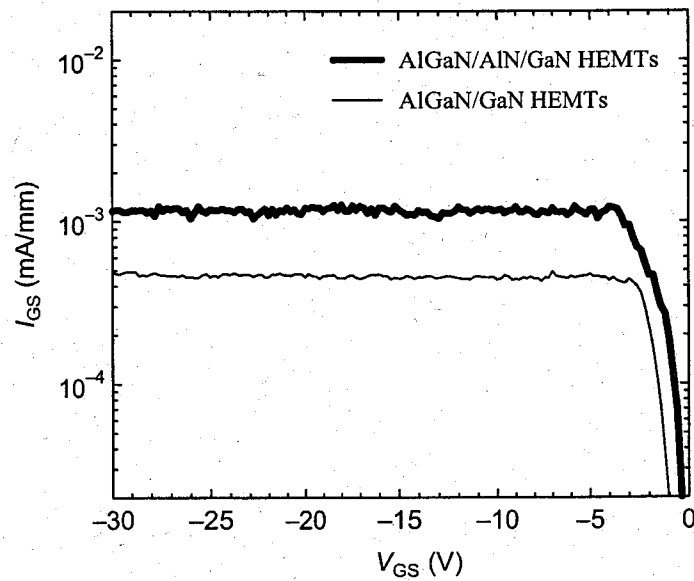


FIG. 4.11. Two-terminal gate-leakage characteristics ($I_{GS}-V_{GS}$) of AlGaN/AlN/GaN and AlGaN/GaN HEMTs grown on sapphire substrates.

Figure 4.11 shows the two-terminal gate-leakage current characteristics ($I_{GS}-V_{GS}$) for AlGaN/AlN/GaN and AlGaN/GaN HEMTs grown on sapphire substrates. From Figure 4.11, I_{GS} for AlGaN/AlN/GaN HEMTs was observed to be approximately two times higher than that for conventional AlGaN/GaN HEMTs. This may imply that a leakage current path was formed in AlGaN layers by the insertion of the thin AlN interfacial layer. Further investigation is, however, needed to understand the gate-leakage properties in AlGaN/AlN/GaN HEMTs.

4.4. Conclusion

In conclusion, we presented a study on mobility enhancement in MOVPE-grown AlGaN/AlN/GaN HEMT structures using 100-mm-diameter sapphire substrates. It was confirmed that a high 2DEG mobility of $1770 \text{ cm}^2/\text{Vs}$ and a low sheet resistance of $365 \text{ } \Omega/\text{sq.}$ with good in-wafer uniformity are obtained for a sample with an optimum AlN layer thickness of 1.0 nm. From the electrical uniformity of MOVPE-grown samples, the thin AlN interfacial layer seemed to be uniformly grown on 100-mm-diameter wafers. Electron transport properties in AlGaN/GaN and AlGaN/AlN/GaN structures were theoretically studied. The calculated results demonstrated that the insertion of an AlN layer into the AlGaN/GaN heterointerface significantly enhances the 2DEG mobility due to the reduction of alloy disorder scattering to the extent that alloy disorder scattering can be neglected.

HEMTs were successfully fabricated and characterized. It was confirmed that AlGaN/AlN/GaN HEMTs show superior DC properties compared with conventional AlGaN/GaN HEMTs. HEMTs based on AlGaN/AlN/GaN structures are very promising candidates for high-frequency electronic devices and/or high-efficiency switching devices and their applications.

References

- [1] I. P. Smorchkova, L. Chen, T. Mates, L. Shen and S. Heikman, B. Moran, S. Keller, S. P. DenBaars, J. S. Speck, and U. K. Mishra, *J. Appl. Phys.* **90**, 5196 (2001).
- [2] L. Shen, S. Heikman, B. Moran, R. Coffie, N. -Q. Zhang, D. Buttari, I. P. Smorchkova, S. Keller, S. P. DenBaars, and U. K. Mishra, *IEEE Trans. Electron Devices* **22**, 457 (2001).
- [3] N. Maeda, T. Tawara, T. Saitoh, K. Tsubaki, and N. Kobayashi, *Phys. Stat. Sol. (a)* **200**, 168 (2003).
- [4] C. X. Wang, K. Tsubaki, N. Kobayashi, T. Makimoto, and N. Maeda, *Appl. Phys. Lett.* **84**, 2313 (2004).
- [5] I. P. Smorchkova, C. R. Elsass, J. P. Ibbetson, R. Vetury, B. Heying, P. Fini, E. Haus, S. P. DenBaars, J. S. Speck, and U. K. Mishra, *J. Appl. Phys.* **86**, 4520 (1999).
- [6] R. Gaska, M. S. Shur, A. D. Bykhovski, A. O. Orlov, and G. L. Snider, *Appl. Phys. Lett.* **74**, 287 (1999).
- [7] G. Y. Xhao, H. Ishikawa, T. Egawa, T. Jimbo, and M. Umeno, *Jpn. J. Appl. Phys. Part 1* **39**, 1035 (2000).
- [8] S. Arulkumaran, M. Sakai, T. Egawa, H. Ishikawa, T. Jimbo, T. Shibata, K. Asai, S. Sumiya, Y. Kuraoka, M. Tanaka, and O. Oda, *Appl. Phys. Lett.* **81**, 1131 (2002).
- [9] L. Hsu and W. Walukiewicz, *J. Appl. Phys.* **89**, 1783 (2001).
- [10] J. Kuzumic: *IEEE Electron Device Lett.* **22**, 510 (2001).
- [11] M. Shur, B. Gelmont, and M. A. Khan, *J. Electron. Mater.* **25**, 777 (1996).
- [12] L. Hsu and W. Walukiewicz, *Phys. Rev. B* **56**, 1520 (1997).
- [13] D. Zanato, S. Gokden, N. Balkan, B. K. Ridley, and W. J. Schaff, *Semicond. Sci. Technol.* **19**, 427 (2004).

- [14] P. Vennéguès, Z. Bougrioua, J. M. Bethoux, M. Azize, and O. Tottereau, *J. Appl. Phys.* **97**, 024912–1 (2005).
- [15] M. Gherasimova, G. Cui, Z. Ren, J. Su, X. L. Wang, J. Han, K. Higashimine, and N. Otsuka, *J. Appl. Phys.* **95**, 2921 (2004).
- [16] Z. Bougrioua, I. Moerman, L. Nistor, B. Van Daele, E. Monroy, E. T. Palacios, F. Calle, and M. Leroux, *Phys. Stat. Sol. (a)* **195**, 93 (2003).

